Chapter 8

Wavelength Calibration (*TTDC*)

High- and low-dispersion small-aperture spectra of the on-board hollow cathode platinum-neon (Pt-Ne) calibration lamp are used to determine wavelength as a function of position in *IUE* images. These wavelength calibration (WAVECAL) exposures were obtained once a month for each camera and are usually a combination of the calibration spectrum and a tungsten flood lamp (TFLOOD) exposure. The TFLOOD exposure was originally added to raise the DN level of the fainter emission lines and was also used to allow reseau marks to be located on the low-dispersion WAVECAL images; these reseau positions were used by IUE-SIPS to perform geometric corrections, but are not needed in the NEWSIPS system. Since approximately mid-1992 WAVECAL images have been obtained without the superimposed TFLOOD exposures, as it was found that the NEWSIPS wavelength calibration analysis was more accurate without them. Instead, the TFLOOD was taken as a separate exposure.

8.1 Image Field-Distortions

Due to residual small-scale geometric distortions introduced by the *IUE* SEC Vidicon cameras, the dispersion solutions for low and high dispersion are not precisely linear in nature. Residuals from a linear fit to the emission-line positions in WAVECAL spectra show significant second- and third-order terms. These distortions lead to wavelength errors on the order of several Ångstroms (low dispersion) or several kilometers per second (high dispersion) in some regions of the camera if left uncorrected. A remapping (along the dispersion direction) of the geometrically-corrected, rotated, linearized, and resampled image (SI) data is necessary to eliminate these distortions and allow the use of a linear dispersion relation. This remapping has been incorporated into the resampling (*GEOM*) step of the image processing system as another vector field that is added to the existing vector fields that describe the image rotation (Chapter 7.1.2) and geometric rectification (Chapter 7.1.3). Higher-order terms, associated with fine scale shifts in the dispersion direction analogous to the fine-scale shifts shown in Figures 7.2 and 7.3, are probably also present but cannot be corrected because of the paucity of WAVECAL Pt-Ne features.

Analysis of many WAVECAL spectra has shown that the first-, second-, and third-order

dispersion terms for low-dispersion SI which have not been linearized are very uniform over time and THDA. This allows the use of a single third-order remapping vector for all low-dispersion images from a given camera. In high dispersion, a similar condition exists except that the remapping vectors are determined separately for each order. The exact form of the correction for each camera is derived as follows. First, a representative sample of WAVECAL images covering the extremes in both observation date and THDA is chosen for analysis. The number of images is typically on the order of 80–90. This sample of images is initially processed without any attempt to apply the (as yet unknown) linearization correction in the *GEOM* step. Third-order Chebyshev dispersion solutions are derived for each of these uncorrected images (using IRAF routines that are described in the next section) and the mean dispersion coefficients for the entire sample are calculated on a term-by-term basis. The mean dispersion coefficients are converted into equivalent pixel-space coefficients, at which point they can be used to compute the appropriate linearization correction vector to apply to all subsequent images within the *GEOM* processing step. The resulting low-dispersion linearization correction displacements for each camera are shown graphically in Figure 7.1. These are included in the *GEOM* processing of every low-dispersion image, so that the SI reflects a linearized wavelength scale. Similar corrections are applied to every order in high dispersion, yielding comparable results.

After the linearization correction is determined for a given camera, all WAVECAL images for that camera are processed with the correction applied (which is the normal processing mode) so that mean linear dispersion solutions and corresponding zeropoint dependencies with time and THDA can be derived as described in the following sections.

8.2 Low-Dispersion Wavelength Calibration

8.2.1 Parameterization of the Dispersion Relations

Each set of calibration images is processed to provide analytic relations between wavelength and pixel position in low-dispersion SI space. The derivation of these dispersion relations is a multi-step process. First, the pixel locations of the Pt-Ne emission lines in a reference low-dispersion WAVECAL image are measured interactively and combined with laboratory values for the wavelength of each emission line (stored in a line library). This analysis is performed using the IRAF task *identify* which generates a dispersion solution that is a one-dimensional fitted function (Chebyshev polynomial) of wavelength versus pixel number. The next step involves the use of the IRAF task *reidentify* which maps the reference-image Chebyshev solution derived from the *identify* step to an ensemble of images. The final dispersion solution is averaged from several hundred individual solutions output from *reidentify* and consists of a starting wavelength and wavelength increment per pixel. The line libraries are based on the Pt-Ne line positions measured by Reader et al. (1990) at the National Institute of Standards and Technology (NIST). Figure 8.1 shows low-dispersion WAVECAL spectra for the LWP/LWR and SWP cameras and indicates the features included in the low-dispersion libraries. Table 8.1 contains listings of the low-dispersion line libraries. The line positions for all cameras, and therefore the dispersion solutions, are expressed in *vacuum* wavelengths.

Because the geometric correction and resampling step of the image processing rotates the low-dispersion images so that the dispersion direction is parallel to the horizontal or x-axis of the low-dispersion SI, the terms of the dispersion solutions for the two image dimensions are completely decoupled. The parameterization of the dispersion solutions is as follows:

$$x = A_1 + A_2\lambda$$

$$y = B_1$$

where x and y are the image pixel locations and A_1, A_2, and B_1 are the dispersion constants. For a low-dispersion SI, the y dimension of the image contains spatial information only. In this case the B_1 coefficient simply gives the image line number at which the spectrum centroid is located.

8.2.2 Application of the Dispersion Relations

The dispersion solutions derived from individual WAVECAL images display variations from the averaged dispersion solutions discussed above. These variations arise from two sources, the first of which is simply the measurement uncertainties involved in locating the Pt-Ne emission features in the WAVECAL images and the corresponding uncertainties in the coefficients of the derived dispersion solutions. Second, global shifts in the location of the spectral format within individual images are known to occur as a function of camera temperature (THDA) and time (see e.g., Thompson 1988 and Garhart 1993). These shifts occur both parallel and perpendicular to the dispersion direction and consequently result in changes

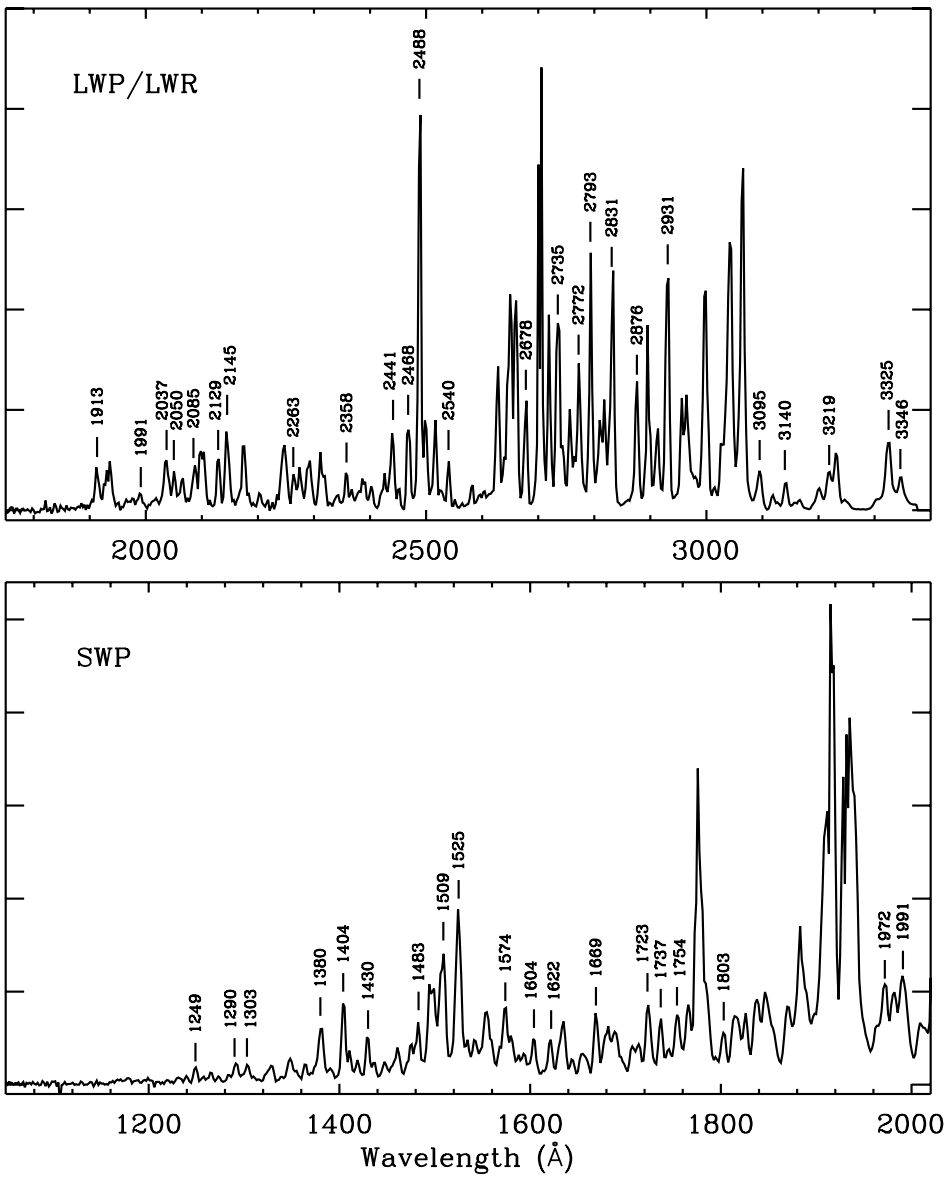

Figure 8.1: Short and long wavelength low-dispersion WAVECAL spectra. Pt-Ne features included in the low-dispersion line libraries are marked.

Table 8.1: Low-Dispersion Pt-Ne Line Libraries

Short Wavelength Camera (Å)	Long Wavelength Cameras (Å)
1248.61	1913.23
1289.95	1990.58
1302.79	2037.12
1380.49	2050.05
1403.90	2085.26
1429.52	2129.31
1482.83	2144.92
1509.29	2263.42
1524.73	2357.83
1574.31	2440.80
1604.01	2468.15
1621.65	2487.92
1669.23	2539.97
1723.13	2677.94
1736.52	2734.77
1753.83	2772.48
1802.94	2792.84
1971.54	2831.13
1990.58	2876.48
	2930.65
	3094.90
	3140.30
	3219.12
	3324.69
	3346.42

to the wavelength zeropoint (A_1) as well as the spatial location (B_1) of spectra within the low-dispersion SI. These format shifts appear to be a translational shift only, with no change in image scale. As a result, the higher order dispersion term (A_2) remains constant.

The dispersion coefficients as actually applied to science images are determined by adding to the mean zeropoint terms corrections appropriate for the observation date and THDA of the particular image. The correction terms W_λ and W_s, which represent the offset that is added to the mean wavelength and spatial zeropoints, are defined by the following general expressions:

$$W_\lambda = W_{1\lambda} + W_{2\lambda}t + W_{3\lambda}T + W_{4\lambda}t^2 + W_{5\lambda}t^3$$

$$W_s = W_{1s} + W_{2s}t + W_{3s}T + W_{4s}t^2 + W_{5s}t^3$$

where W_λ and W_s are the corrections to be added to the A_1 and B_1 terms of the mean dispersion relation, respectively, T is the THDA at the end of exposure, and t is time expressed as the total number of elapsed days since 1 January 1978.

A first-order (i.e., linear) fit is sufficient to characterize the correlation between THDA and zeropoint for all cameras. The correlation between time and zeropoint, however, has second- and third-order dependencies for some cameras. The W_λ and W_s coefficients in use for the low-dispersion mode for pre-1990 LWP and SWP images are listed in Table 8.2. Coefficients appropriate for more recent LWP and SWP images are discussed in Chapter 8.2.3. The database of exposures used to generate the coefficients in Table 8.2 include WAVECAL images obtained through mid-1993 for the LWP and mid-1991 for the SWP. The respective coefficients for the LWR camera are listed in Table 8.3. In the case of the LWR, a separate set of coefficients are tabulated for the ITF A and ITF B calibrations. In addition, each ITF has an early and late epoch. This is due to the fact that the wavelength zeropoint shift was dramatically different between these two epochs. The cutoff date for the early and late epochs is 1980.1 for ITF A and 1979.9 for ITF B. The shift of the spectrum center does not exhibit this trend, so the spatial coefficients are identical for each epoch. The zeropoint shifts and corresponding polynomial fits are illustrated graphically for each camera in Figures 8.2–8.5.

8.2.3 1995 Wavelength Calibration Updates

In early 1995, concerns were raised about the accuracy of the extrapolations of the low-dispersion wavelength calibrations (i.e., the time and THDA wavelength and spatial zeropoint dependencies) to times beyond the original database of observations. While no errors due to the extrapolated corrections were seen in NEWSIPS data, the *IUE* Project felt that updating the old wavelength calibration analysis would result in more accurate wavelengths for recent LWP and SWP images. As a result of these concerns, the LWP and SWP wavelength calibration analysis was updated in 1995 using data taken though the beginning of 1995. These new corrections were applied to post-01 January 1990 images while the old corrections were used for pre-1990 images. No calibration update was required for the LWR camera, as it comprised a closed data set. The updated coefficients are listed in Table 8.4.

Table 8.2: LWP and SWP Low-Dispersion Time and THDA Coefficients (pre-1990)

	LWP	SWP
A_1 (Å)	1711.6597	1032.4392
A_2 (Å/pix)	2.6626680	1.6763376
B_1 (pix)	23.61	21.97
$W_{1\lambda}$	4.4345033	−2.3252555
$W_{2\lambda}$	4.0537516e−4	3.5285037e−3
$W_{3\lambda}$	−6.0635105e−1	−2.6882430e−1
$W_{4\lambda}$	0.0	−6.1677609e−7
$W_{5\lambda}$	0.0	4.2678509e−11
W_{1s}	−4.3763553	4.3991865
W_{2s}	2.8160580e−4	−3.2833262e−3
W_{3s}	3.6686645e−1	−1.0900706e−1
W_{4s}	0.0	8.2522805e−7
W_{5s}	0.0	−7.1718122e−11

Table 8.3: LWR Low-Dispersion Time and THDA Coefficients

	LWR ITF A		LWR ITF B	
	Pre-1980.1	Post-1980.1	Pre-1979.9	Post-1979.9
A_1 (Å)	1730.1170	1730.7719	1727.5143	1728.2415
A_2 (Å/pix)	2.6658213	2.6657266	2.6692838	2.6688933
B_1 (pix)	24.78	24.78	25.04	25.04
$W_{1\lambda}$	10.1020149	−4.7995158e−1	9.2690908	−2.0569484e−1
$W_{2\lambda}$	−1.6612805e−2	2.9549095e−3	−1.5753037e−2	2.5944874e−3
$W_{3\lambda}$	−4.5748750e−1	−2.4267995e−1	−4.1245027e−1	−2.2761587e−1
$W_{4\lambda}$	1.6308716e−5	−6.2727972e−7	1.5803093e−5	−6.0699193e−7
$W_{5\lambda}$	−4.5832944e−9	4.2171131e−11	−4.5624765e−9	5.1719073e−11
W_{1s}	−11.6908924	−11.6908924	−11.5273270	−11.5273270
W_{2s}	2.9216646e−3	2.9216646e−3	3.0038018e−3	3.0038018e−3
W_{3s}	6.1467118e−1	6.1467118e−1	5.9936489e−1	5.9936489e−1
W_{4s}	−5.9403908e−7	−5.9403908e−7	−6.2260391e−7	−6.2260391e−7
W_{5s}	4.1402462e−11	4.1402462e−11	4.3818172e−11	4.3818172e−11

Table 8.4: LWP and SWP Low-Dispersion Time and THDA Coefficients (post-1990)

	LWP	SWP
A_1 (Å)	1711.7219	1032.7897
A_2 (Å/pix)	2.6627994	1.6763867
B_1 (pix)	23.66	21.97
$W_{1\lambda}$	3.1902447	−2.6142797
$W_{2\lambda}$	1.2511673e−3	3.4473210e−3
$W_{3\lambda}$	−6.2114623e−1	−2.7509139e−1
$W_{4\lambda}$	−1.2237954e−7	−5.6468763e−7
$W_{5\lambda}$	0.0	3.43165905−11
W_{1s}	−4.4882965	4.6596390
W_{2s}	2.7621062e−4	−3.2043927e−3
W_{3s}	3.7540199e−1	−1.1149894e−1
W_{4s}	0.0	8.0137016e−7
W_{5s}	0.0	−7.1156480e−11

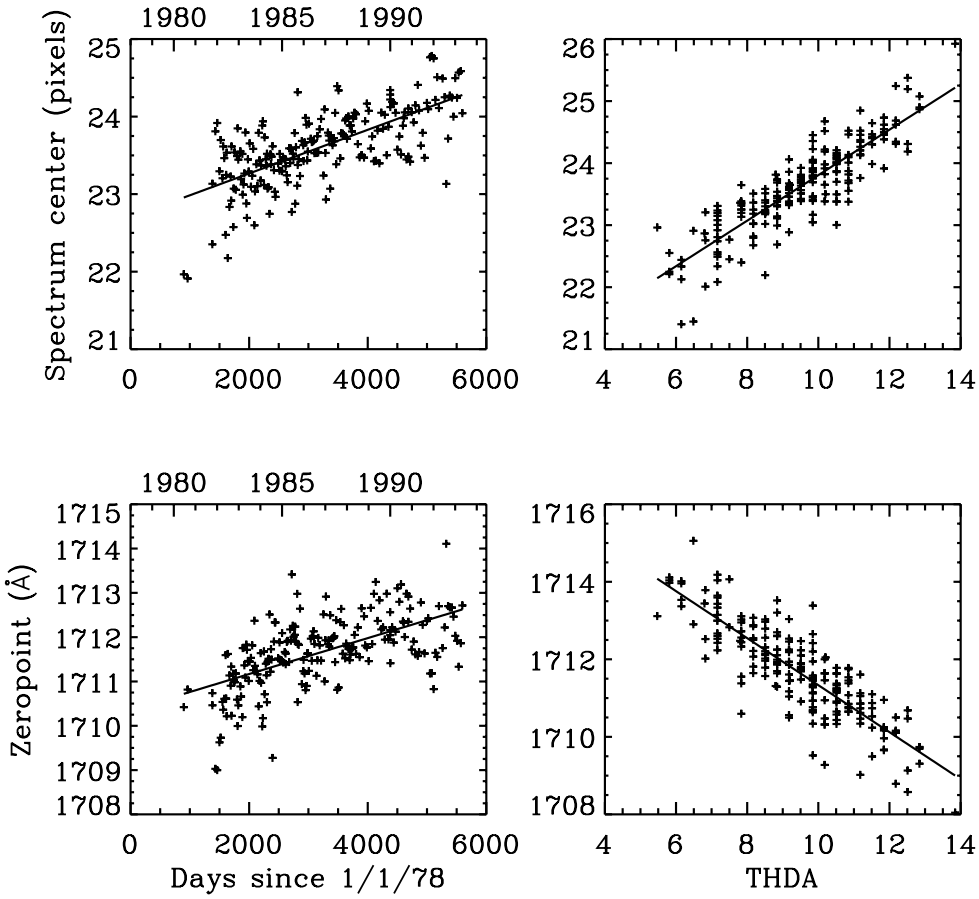

Figure 8.2: Low-dispersion time and temperature correlations with wavelength and spatial zeropoints for the LWP camera.

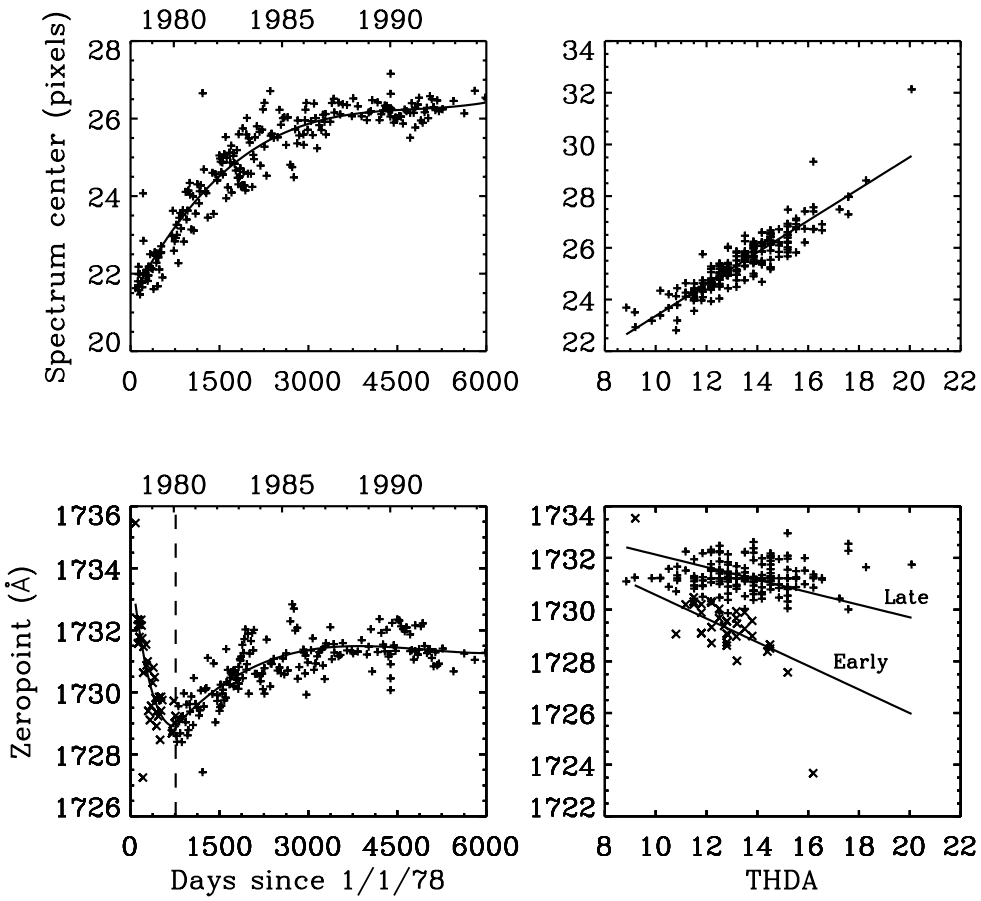

Figure 8.3: Low-dispersion time and temperature correlations with wavelength and spatial zeropoints for the LWR camera (ITF A).

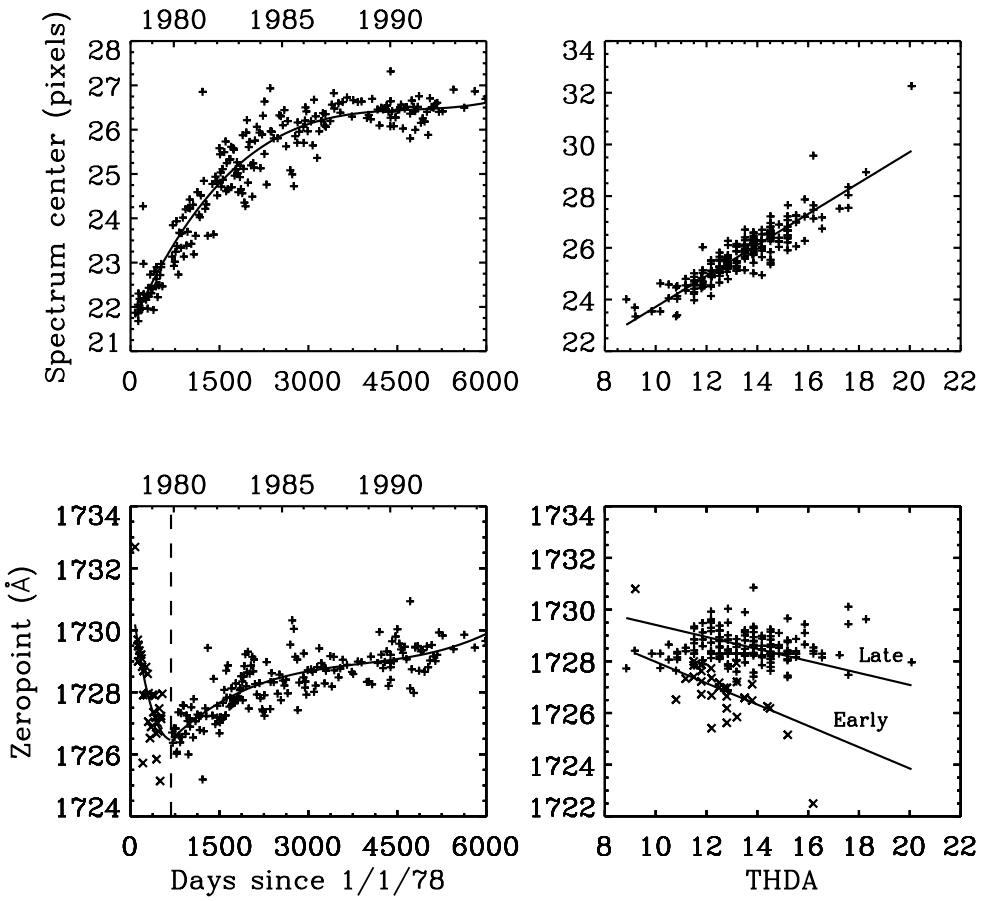

Figure 8.4: Low-dispersion time and temperature correlations with wavelength and spatial zeropoints for the LWR camera (ITF B).

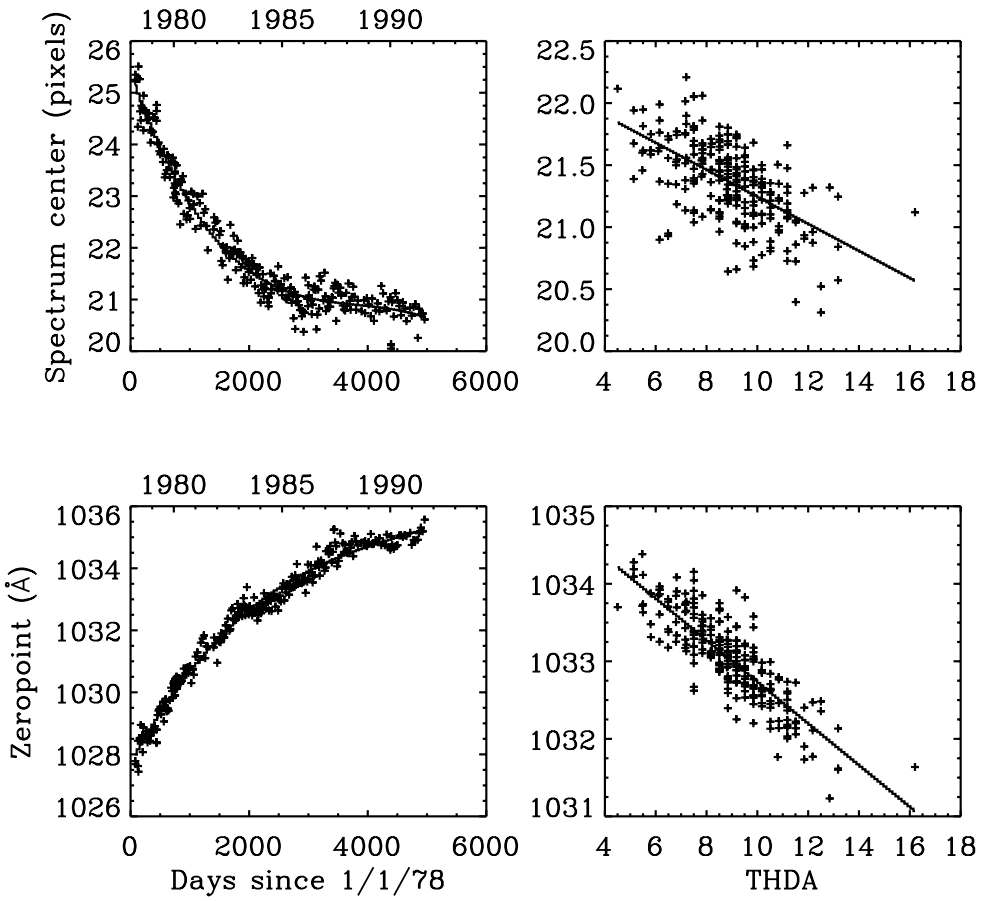

Figure 8.5: Low-dispersion time and temperature correlations with wavelength and spatial zeropoints for the SWP camera.

8.3 High-Dispersion Wavelength Calibration

8.3.1 Parameterization of Dispersion Relations

The separation of the echelle orders in the spatial direction by the cross-disperser complicates the calculation of the wavelength parameterization of high-dispersion *IUE* spectra. NEWSIPS departs from IUESIPS in seeking a 1:1 correspondence between dispersion parameters and physical properties of the spectro-optical system. The goal of such a representation is to identify each term with optical properties of the spectrograph and to prevent these physical effects from introducing cross-terms that could complicate the estimate of errors in the wavelength solution (for a full discussion of this concept, see Smith 1990a, 1990b). In the raw geometry this is not possible because the rotation of the order produces a correlation of the line and sample positions for a wavelength. For low-dispersion images this problem is largely solved by de-rotating the image. In the high-dispersion geometry the dispersion axis is also dependent on the echelle order: the precise angle is equal to the tangent of the dispersing powers of the echelle and cross-dispersing grating. Because this factor varies as $1/m_{ech}$, the dispersion axis slowly rotates and produces a splaying of the orders (see Chapter 7.3.1). In order to place all echelle orders along a common pseudo-dispersion axis, the order-splaying is removed as part of a single resampling step in the *GEOM* module. This removes the second and last of the important cross-coupling terms between the two axes in the original raw space. Thus the *GEOM* resampling forces the echelle orders to fall along a common *sample* axis (s) and to be separated by a difference in *line* positions (l) on the high-dispersion SI. This operation produces a small tilt of a monochromatic image on an order which is usually ignored because its effect on the spectral instrumental profile is small.

The representation of the dispersion parameters in the rectilinear (s, l) high-dispersion SI geometry can be expressed as a Taylor expansion of the grating equation in terms of the quantity $m_{ech}\lambda$. The equations for the dispersion solution for sample and line positions are:

$$s = A_1 + A_2(\lambda m_{ech}/m_{Xdisp}) + A_3(\lambda m_{ech}/m_{Xdisp})^2 + ..., \quad (8.1)$$

$$l = B_1 + B_2(\lambda m_{Xdisp}/m_{ech}) + B_3(\lambda m_{Xdisp}/m_{ech})^2 + ..., \quad (8.2)$$

where the m's refer to the order numbers for the echelle and cross-dispersing gratings (m_{Xdisp} = 1) and the A's and the B's are constants to be determined empirically. The relations in Equations 8.1 and 8.2 represent an orthogonal system (i.e., each of the factors is decoupled from the others).

In practice higher-order terms in the Taylor expansion of the dispersion solution are small for the *IUE* gratings and need not be considered. However, the quadratic term is still significant for the *IUE* grating geometry (Smith 1990a, 1990b). Furthermore, although the cubic and quartic terms are not significant in the Taylor expansion of the grating equation, such terms *do* arise from the electro-optical distortions within the *IUE* cameras. These high-order terms (quadratic, cubic, and quartic) have been determined empirically as a function of echelle order and incorporated within the *GEOM* module as additional terms, as in the linearization process performed in low dispersion (Chapter 8.1). The result of these *GEOM*

corrections is an SI with very nearly linear relation between wavelength and sample position in each order.

8.3.2 Calculation of the Dispersion Coefficients

As is the case in low dispersion, each set of high-dispersion WAVECAL images is processed to provide the relation between wavelength and pixel position. The analytic method is also the same multi-step process as used in low dispersion; it simply has been expanded to include a group of echelle orders rather than one single order. The high-dispersion line libraries are based on an updated set of Pt-Ne line positions measured by Sansonetti et al. (1992) at the NIST. The line positions for all cameras, and therefore the dispersion solutions, are expressed in *vacuum* wavelengths.

The linear mapping of high-dispersion images from pixel space to Ångstroms was carried out with the *IRAF* routine *identify*. This task identifies the emission lines for a single order in a reference WAVECAL spectrum and generates a dispersion solution which is a one-dimensional fitted function (Chebyshev polynomial) of wavelength versus pixel number. The next step involves the use of the IRAF task *reidentify* which maps the reference-image Chebyshev solution derived from the *identify* step to an ensemble of images. The final dispersion solution for a given order is averaged from several hundred individual solutions output from *reidentify* and consists of a starting wavelength and wavelength increment per pixel. This process is repeated for every order to yield a set of order-by-order solutions.

Some orders, particularly those at the shorter wavelengths, have too few Pt-Ne lines in the WAVECAL spectra for valid individual dispersion solutions. In these cases the IRAF tasks *ecidentify* and *ecreidentify* were used to determine two-dimensional dispersion solutions (as a function of wavelength and order number versus pixel) for a specified block of orders; thus the Chebyshev solutions for these orders are coupled. The types of IRAF solutions used for the wavelength linearization and the time and temperature correlation steps are listed in Tables 8.5 and 8.6. The block solution simultaneously solves for three contiguous orders and is applied only to the central order of the block. The global solution solves for all orders and usually is utilized only (with the exception of the LWR) for the higher orders.

Table 8.5: IRAF Solutions Used for the Wavelength Linearization Step

Method	LWP	LWR	SWP
Order by Order	69,70,72, 73,75–102	67,72,73,75–82, 85–96,98	66–101
Block	71,74	71,97,99	
Global	103–127	68–70,74,83, 84,100–127	102–125

Table 8.6: IRAF Solutions Used for Time and Temperature Correlation Step

Method	LWP	LWR	SWP
Order by Order	69,70,72	67,68,71,73,	66–101
	73,75–109	75,76,78–82	
Block	71,74	72,77,93–99	
Global	110–127	69,70,74,83,	102–105
		84,90,100–127	

8.3.3 Time and THDA Dependence of the Wavelength Zeropoint

Once the mean dispersion solutions were derived from typically several hundred images, the wavelength zeropoint motion was determined as a function of time and THDA. Mean time- and THDA-dependent coefficients were determined, as in low-dispersion, permitting predicted zeropoint shifts (one value for each order of an image) to be evaluated from these relations. Typically fourth-order polynomials are used to represent the variation in the wavelength system as a function of time, while the THDA dependence is represented by a linear function. The time- and THDA-predicted zeropoint shifts in the wavelength direction are applied to every image. The time- and THDA-predicted zeropoint shifts in the spatial direction are applied *only* in cases where empirically-measured registration shifts cannot be successfully determined by the order registration algorithm within the *RAW_SCREEN* function (see Chapter 4.9).

8.3.4 Checks Against Other Calibrations

A check of the SWP high-dispersion wavelength calibration was made against the *Copernicus* satellite wavelength system for the standard B0.2 τ Scorpii with representative large-aperture images. This check showed a zeropoint offset of -4 km/s with respect to the *Copernicus* system for typical images; no trend with wavelength was found. The estimated errors in the *IUE* wavelengths as measured from these τ Scorpii observations were ± 5 km/s per line.

8.3.5 Pertinent Spectrograph Parameters

Table 8.7 contains further spectrographic lay-out and design information which has bearing on spectroscopic behavior for the three *IUE* cameras. The echelle grating and cross-disperser parameters are taken from Boggess et al. (1978), Evans (1975), and the *IUE* System Design Report (1976). These values are believed to be accurate, except that there is evidence that the effective focal lengths of the cameras were modified by several percent during the instrument assembly and testing stages.

The approximate wavelength ranges for each order are listed in Table 8.8. These values

Table 8.7: *IUE* Spectrograph Parameters

Parameter	LWP	LWR	SWP
Wavelength Range (Å)	1808–3359	1810–3456	1097–2097
Order Range	69–127	67–127	66–125
Abs. Calib. Wavelength Range (Å)	1850–3350	1850–3350	1150–1980
Abs. Calib. Order Range	69–125	69–125	70–120
Coll. Focal Length (mm)	950	950	950
Cam. Focal Length (mm)	684	684	684
Coll.-to-Cam. Angle (deg.)	20.42	20.42	20.37
Image Scale (μm pix^{-1})	36.4	36.4	35.7
X-Disp. Ruling Freq. (gr mm^{-1})	241.50	241.50	369.233
X-Disp. Order	1	1	1
Ech. Ruling Freq. (gr mm^{-1})	63.207	63.207	101.947
Ech. Blaze Wavel. (μm)	23.19	23.19	13.76
Ech. Blaze Angle β (deg.)	48.126	48.126	45.449
Ech. Grating Angle ϕ (deg.)	0	0	0

will vary by several tenths of an Ångstrom due to the global shifts in the location of the spectral format as a function of time and THDA.

A few remarks concerning the spectrographic elements:

- the collimator mirror is an off-axis paraboloid,
- the camera mirror is ruled as the cross-dispersing element,
- the echelle grating operates in a Littrow mode,
- the separation of the incoming and outgoing rays at the grating is achieved in the direction perpendicular to the dispersion (i.e., the echelle operates in an "over-under Littrow mode"),
- differences in the dispersion caused by the angular separation between the large and small entrance apertures are <0.1% and are not detectable.

Note finally that the wavelength coverage for the long wavelength cameras, particularly for the LWR, extends into the accessible range of ground-based instruments. The long-wavelength limits for absolutely calibrated fluxes for all three cameras is limited by the low-dispersion spectra impinging on the camera target ring.

Table 8.8: Approximate Wavelength Ranges for the Echelle Orders - continued on next page

Order	LWP		LWR		SWP	
No.	Large	Small	Large	Small	Large	Small
127	1808.9–1830.6	1809.9–1831.9	1811.6–1830.5	1811.5–1831.7		
126	1823.1–1845.2	1824.0–1846.7	1824.4–1845.4	1825.6–1846.7		
125	1850.0–1860.2	1850.0–1861.3	1850.2–1860.4	1850.0–1861.8	1098.1–1112.6	1097.3–1112.0
124	1852.0–1875.1	1853.1–1876.9	1853.3–1875.8	1854.5–1877.1	1106.8–1121.6	1106.0–1121.0
123	1866.8–1891.0	1867.9–1892.4	1868.3–1891.2	1869.3–1892.6	1115.7–1130.9	1114.9–1130.3
122	1881.9–1906.7	1883.0–1908.0	1883.2–1906.9	1884.4–1908.9	1124.7–1140.3	1123.9–1139.7
121	1897.3–1922.7	1898.3–1924.0	1900.0–1923.0	1901.2–1924.3	1133.8–1149.8	1133.1–1149.2
120	1912.8–1938.9	1913.9–1940.3	1915.8–1939.2	1915.4–1940.5	1150.0–1157.8	1150.0–1158.0
119	1928.7–1955.4	1929.7–1956.8	1930.0–1955.5	1931.3–1957.1	1152.6–1167.6	1151.7–1167.7
118	1944.7–1972.2	1946.3–1973.5	1946.2–1972.6	1947.4–1974.0	1162.2–1177.6	1161.4–1177.7
117	1961.7–1989.2	1962.3–1990.6	1962.6–1989.6	1963.9–1991.0	1172.0–1187.7	1171.2–1187.8
116	1977.9–2006.6	1979.1–2008.0	1979.3–2007.0	1980.6–2008.4	1181.9–1197.8	1181.2–1198.1
115	1994.9–2024.2	1996.1–2025.6	1996.3–2023.9	1997.6–2026.1	1192.0–1208.5	1191.3–1208.6
114	2012.2–2042.1	2013.4–2043.5	2015.0–2041.7	2016.1–2044.0	1202.3–1219.1	1201.6–1219.2
113	2029.8–2060.4	2031.0–2061.8	2032.8–2060.8	2032.6–2062.2	1213.7–1230.1	1212.1–1230.1
112	2047.7–2079.0	2049.0–2080.4	2049.2–2079.4	2050.5–2080.9	1224.5–1241.0	1222.8–1241.1
111	2065.0–2097.9	2067.3–2099.3	2067.5–2098.4	2068.8–2099.8	1234.5–1252.3	1233.7–1252.4
110	2084.7–2117.1	2085.9–2118.5	2086.1–2117.6	2087.5–2119.1	1245.6–1263.7	1244.8–1263.8
109	2103.6–2136.7	2104.8–2138.1	2105.1–2137.2	2106.4–2138.7	1256.9–1275.4	1256.1–1275.5
108	2122.9–2155.5	2124.2–2156.7	2124.4–2157.2	2126.7–2158.8	1268.4–1287.3	1267.6–1287.4
107	2142.6–2175.6	2143.9–2178.3	2145.2–2177.5	2146.4–2179.0	1280.1–1299.4	1279.8–1299.5
106	2162.4–2197.6	2163.9–2198.9	2164.2–2198.2	2165.6–2199.7	1292.7–1311.7	1291.3–1311.8
105	2183.0–2218.7	2184.4–2220.0	2184.6–2219.4	2186.0–2220.6	1304.3–1323.6	1303.5–1324.4
104	2203.9–2239.9	2205.2–2241.5	2205.5–2240.9	2206.9–2242.3	1316.7–1337.1	1316.0–1337.2
103	2225.2–2261.8	2226.6–2263.5	2226.7–2262.8	2228.2–2264.2	1329.4–1350.2	1328.7–1350.3
102	2246.9–2284.0	2248.1–2285.4	2248.4–2285.1	2249.9–2286.6	1342.4–1363.5	1341.6–1363.6
101	2269.0–2306.6	2270.4–2308.0	2270.6–2307.5	2272.0–2309.0	1355.6–1377.1	1354.8–1376.8
100	2291.4–2329.8	2292.9–2331.3	2293.2–2330.6	2294.7–2332.6	1369.1–1391.0	1368.3–1391.1
99	2314.5–2353.4	2316.0–2353.2	2316.2–2353.5	2317.7–2355.0	1382.8–1405.0	1382.0–1405.3
98	2338.0–2375.6	2339.4–2379.0	2339.7–2378.9	2341.8–2380.5	1396.9–1418.9	1396.1–1419.7
97	2362.0–2402.1	2363.4–2403.7	2363.9–2403.5	2365.4–2405.1	1411.2–1434.3	1410.4–1434.4

Table 8.8: Approximate Wavelength Ranges for the Echelle Orders - continued

Order	LWP		LWR		SWP	
No.	Large	Small	Large	Small	Large	Small
96	2387.0–2427.2	2388.5–2428.7	2388.3–2428.6	2389.9–2430.3	1425.8–1449.4	1425.0–1449.5
95	2411.5–2452.7	2412.9–2454.3	2413.6–2454.3	2415.1–2455.9	1440.8–1463.2	1440.0–1464.9
94	2437.2–2478.8	2438.7–2480.4	2439.0–2480.5	2440.6–2482.1	1456.1–1480.5	1455.3–1480.6
93	2463.4–2505.4	2464.9–2507.0	2466.7–2507.2	2466.9–2508.3	1471.7–1496.5	1470.9–1496.6
92	2490.0–2532.6	2491.6–2534.2	2492.0–2533.6	2493.6–2536.0	1488.3–1512.7	1487.5–1511.9
91	2517.3–2560.5	2518.9–2560.5	2519.3–2562.2	2521.0–2563.5	1504.0–1529.7	1503.2–1529.8
90	2545.4–2588.8	2547.0–2590.4	2547.4–2590.5	2549.1–2592.3	1520.7–1546.8	1519.9–1546.9
89	2574.1–2617.8	2576.6–2619.4	2576.0–2619.8	2577.7–2621.4	1537.8–1564.4	1536.9–1564.5
88	2604.3–2647.4	2605.0–2649.0	2605.4–2649.5	2607.1–2651.2	1555.3–1582.3	1554.4–1582.4
87	2633.5–2677.7	2635.1–2679.3	2635.4–2680.0	2637.1–2681.5	1573.2–1600.6	1572.3–1600.8
86	2664.2–2708.6	2666.0–2710.2	2668.3–2711.0	2669.8–2712.6	1591.6–1619.4	1590.7–1619.5
85	2695.7–2740.6	2697.5–2742.0	2697.8–2742.9	2699.5–2744.5	1610.4–1638.6	1610.6–1636.7
84	2727.9–2772.5	2729.8–2774.1	2731.8–2775.3	2733.5–2777.0	1630.4–1657.0	1628.7–1658.0
83	2761.1–2805.8	2762.9–2807.5	2763.2–2808.4	2765.0–2810.2	1649.3–1678.5	1648.4–1677.8
82	2795.5–2839.3	2797.3–2841.3	2797.3–2842.3	2799.1–2843.0	1669.6–1699.0	1668.6–1669.5
81	2830.1–2874.2	2831.9–2875.9	2832.0–2877.3	2833.9–2879.1	1690.5–1719.8	1689.6–1718.9
80	2865.8–2909.7	2867.7–2911.3	2869.1–2912.9	2870.9–2914.6	1711.8–1741.2	1710.9–1740.3
79	2902.6–2946.0	2904.5–2947.6	2904.5–2949.2	2906.4–2950.7	1733.7–1763.0	1732.8–1762.0
78	2940.3–2982.9	2942.3–2984.6	2942.2–2986.3	2944.1–2988.0	1756.4–1784.9	1755.4–1784.3
77	2979.2–3020.7	2981.3–3022.3	2980.9–3024.6	2982.9–3026.5	1779.3–1808.2	1778.3–1807.1
76	3019.2–3059.5	3021.3–3061.2	3020.9–3063.6	3022.8–3065.4	1803.0–1831.6	1803.5–1830.5
75	3060.3–3099.4	3062.6–3101.2	3061.9–3103.7	3066.4–3105.7	1827.4–1854.6	1826.5–1853.7
74	3102.5–3140.3	3105.0–3142.1	3104.3–3144.9	3106.8–3146.8	1852.6–1880.2	1851.7–1879.2
73	3146.7–3182.0	3148.9–3183.4	3148.8–3187.4	3150.6–3189.3	1878.5–1905.4	1877.6–1904.2
72	3191.9–3224.6	3194.2–3225.5	3193.0–3230.0	3195.3–3232.1	1905.3–1931.2	1904.4–1930.0
71	3237.4–3267.0	3239.5–3268.9	3240.8–3273.4	3242.8–3275.8	1932.9–1957.7	1931.9–1956.5
70	3287.8–3311.7	3290.2–3312.6	3287.9–3318.3	3290.2–3320.4	1961.5–1980.0	1960.5–1980.0
69	3338.8–3348.2	3342.2–3349.9	3338.3–3350.0	3340.7–3349.9	1990.9–2012.4	1989.9–2011.2
68			3390.7–3410.0	3393.5–3411.4	2021.5–2040.7	2020.6–2039.3
67			3444.3–3456.5	3446.5–3458.7	2053.5–2069.2	2052.6–2067.6
66					2087.4–2097.7	2086.3–2096.1

8.4 *TTDC* Output

The *TTDC* module does not generate any output data products (i.e., FITS file). Instead it produces a temporary (internal only) file which contains various spatial- (in the case of low dispersion) and wavelength-dependent parameters that are used by subsequent processing modules (e.g., *GEOM*).

8.4.1 Low-Dispersion

The *TTDC* module writes the following information to the HISTORY portion of the low-dispersion image label:

- THDA used for correcting dispersion constants,
- date of observation used for correcting dispersion constants,
- degree of time-dependent polynomial fit,
- degree of THDA-dependent polynomial fit,
- zeropoint correction in Ångstroms, and
- spatial correction in pixels.

8.4.2 High-Dispersion

The *TTDC* module writes the following information to the HISTORY portion of the high-dispersion image label:

- THDA used for correcting dispersion constants,
- date of observation used for correcting dispersion constants,
- zeropoint correction in Ångstroms for each order,
- spacecraft velocity vector,
- Earth velocity vector,
- net (spacecraft + Earth) correction vector to heliocentric velocity, and
- heliocentric velocity correction in kilometers per second.